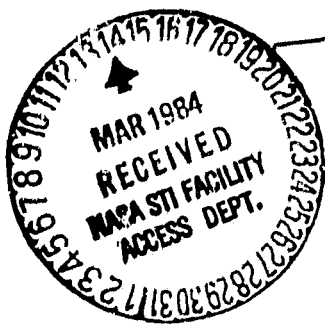


General Disclaimer

One or more of the Following Statements may affect this Document

- This document has been reproduced from the best copy furnished by the organizational source. It is being released in the interest of making available as much information as possible.
- This document may contain data, which exceeds the sheet parameters. It was furnished in this condition by the organizational source and is the best copy available.
- This document may contain tone-on-tone or color graphs, charts and/or pictures, which have been reproduced in black and white.
- This document is paginated as submitted by the original source.
- Portions of this document are not fully legible due to the historical nature of some of the material. However, it is the best reproduction available from the original submission.



DPA

LMSC-HREC TR D951333

MANUFACTURING IN SPACE: FLUID DYNAMICS NUMERICAL ANALYSIS

February 1984

Contract NASW-3281 (Final Report)

(NASA-CR-175401) MANUFACTURING IN SPACE:
FLUID DYNAMICS NUMERICAL ANALYSIS Final
Report, Jan. 1983 - Jan. 1984 (Lockheed
Missiles and Space Co.) 38 p HC A03/MF A01

N84-19748

Unclas
CSCL 20D G3/34 18702

Prepared for

**NASA HEADQUARTERS
WASHINGTON, DC 20546**

by

S. J. Robertson



*Missiles & Space Company, Inc.
Huntsville Research & Engineering Center*

4800 Bradford Drive, Huntsville, AL 35807

FOREWORD

This document is the final report describing the results of effort by personnel of Lockheed Missiles & Space Company, Inc., Huntsville Research & Engineering Center, for the National Aeronautics and Space Administration under Contract NAS8-3281, "Fluid Dynamics Numerical Analysis." The contractual effort described in this document was performed during the year from January 1983 to January 1984. The NASA Technical Director for this contract is Dr. William Oran, NASA Headquarters, Washington, D.C.

ACKNOWLEDGMENT

The work described in this document was done in coordination with a research program conducted by Dr. Robert F. Dressler of George Washington University. We greatly appreciate his suggestions and assistance during the course of the current contractual effort, and during the previous years that we have been associated since this work was initiated in 1979.

PRECEDING PAGE BLANK NOT FILMED

CONTENTS

	<u>Page</u>
FOREWORD	ii
ACKNOWLEDGMENT	ii
INTRODUCTION AND SUMMARY	1
DISCUSSION	2
CONCLUSIONS	11
REFERENCES	12
TABLE AND FIGURES	13
APPENDIX: Simplified Analytical Model for Estimating Marangoni Convection in Square Enclosures	A-1

INTRODUCTION AND SUMMARY

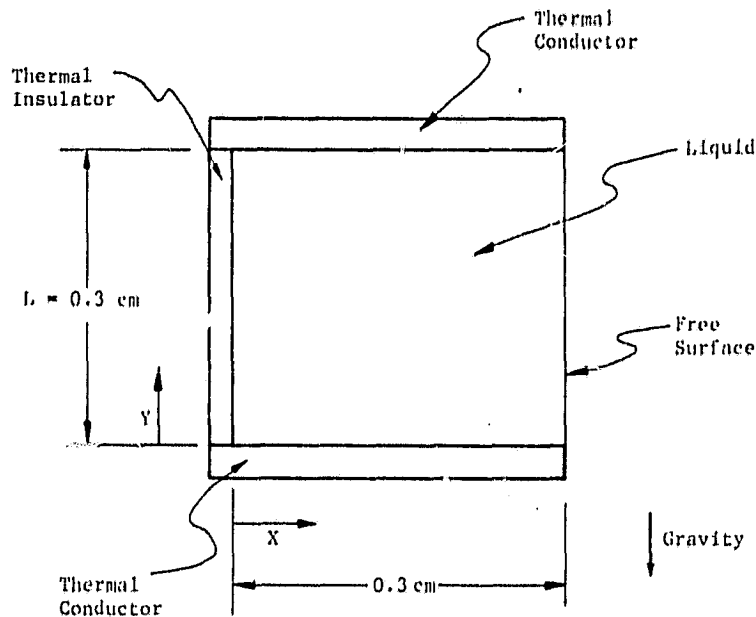
The research program described in this final report is a continuation of effort initiated in August 1979 to investigate natural convection in various materials processing experiment configurations under microgravity conditions simulating the orbiting Space Station environment. In the years since this research program was initiated, a number of microgravity natural convection problems have been investigated, including the upper limit on Rayleigh number for linear (low Rayleigh number) theory to be valid, the effect of container shape on convection velocities, and the effect of changes in the microgravity vector (direction and magnitude) on convection velocities. In addition, the development of natural convection was simulated in the Lal/Kroes experiment. These results are described in annual reports for this contract (Refs. 1 through 3).

The results described in this document are for the period from January 1983 to January 1984. During this period, the effort was concerned primarily with numerically simulating thermocapillary convection in Dr. Robert F. Dressler's air-jet Marangoni flow suppressing technique. Dr. Dressler, of George Washington University, is developing this technique under a separate NASA contract. In cooperation with Dr. Dressler, we performed numerical simulations for flow under various conditions of fluid properties, gravity, and temperature gradient. Results presented herein include computer generated plots of streamlines, velocities, and temperatures throughout the contained fluid flow, and plots of Marangoni flow velocities over the free surface.

ORIGINAL PAGE IS
OF POOR QUALITY

DISCUSSION

Thermocapillary convection was simulated for flow in the idealized two-dimensional container illustrated in the following sketch. The container is



Idealized Two-Dimensional Square Container
for Thermocapillary Flow Simulation

square-shaped with the interior dimensions $0.3 \text{ cm} \times 0.3 \text{ cm}$. The top and bottom of the container are perfect thermal conductors held at constant temperatures, with the top at a temperature, ΔT , greater than the bottom. One side of the container is a perfect thermal insulator, and the other side is open, so that the liquid surface on that side is free. For these numerical simulations, we assume that the liquid free surface is always flat. We also assume that there is no heat transfer across the liquid free surface. Where gravity is present, the direction is always downward.

ORIGINAL PAGE IS
OF POOR QUALITY

A simplified analysis was performed to develop closed form algebraic equations approximately relating fluid velocities with the various experimental parameters. This was done to provide initial estimates for selecting experimental conditions to be numerically simulated. A brief description of the development of these simplified equations is given in the appendix. The maximum fluid velocity, v_{\max} , at steady state is given by

$$v_{\max} = \frac{\tau_w L}{4\mu} \quad (1)$$

where τ_w is the surface shear caused by surface tension gradient, L is the length of the side of the square enclosure and μ is viscosity. The surface shear τ_w is given by

$$\tau_w = \frac{d\sigma}{dT} \frac{dT}{dy} \approx \frac{\Delta T}{L} \quad (2)$$

where $d\sigma/dT$ is the surface tension temperature coefficient and ΔT is the temperature difference across the free surface.

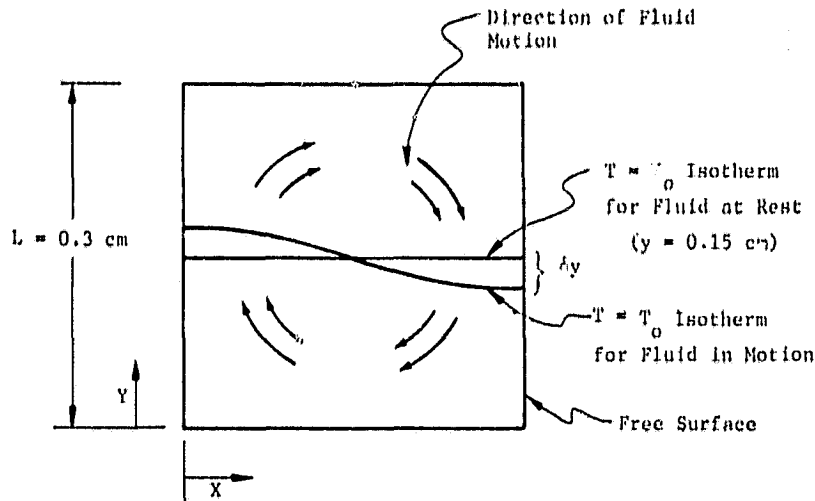
The equilibrium temperature distribution for the fluid-at-rest consists of straight-line isotherms parallel to the x axis. The distortion, δy , in the isotherms due to fluid motion is given by

$$\frac{\delta y}{L} = \frac{1}{12 + \pi^2} \frac{v_{\max} L}{\alpha} \quad (3)$$

where α is the thermal diffusivity. The distortion δy is the displacement of the $T = T_0$ isotherm from the $y = 0.15$ cm line at the free surface (see sketch, next page).

Some type of silicone oil was originally intended for use in the experimental program. Silicone oils are available in a wide range of

ORIGINAL PAGE 19
OF POOR QUALITY



Schematic Showing Displacement of Isotherm
Due to Fluid Motion

viscosity grades. The salient properties of Dow Corning 200 fluid (Ref. 4) are listed in Table 1. These listed properties are essentially the same regardless of the viscosity grade. The surface tension temperature coefficient was provided by Dr. Dressler.

In order to permit reasonable accuracy in the experimental measurements, the temperature difference ΔT across the fluid was required to be at least 1 C and the free surface fluid velocity at least 1 mm/sec. The first set of conditions that we considered was for $\Delta T = 5 \text{ C}$ using 1000 centistoke viscosity fluid. The surface shear, τ_w , for this temperature difference was estimated from Eq. (2) to be about -1.0 dyne/cm^2 . The maximum fluid free surface velocity v_{max} was then estimated from Eq. (1) to be about -0.07 mm/sec (flowing downward), considerably less than the 1 mm/sec minimum

in our experimental guidelines. The displacement of the isotherms was estimated from Eq. (3) to be approximately 8 percent of the distance across the free surface. This indicates that the temperature distribution across the free surface should not be perturbed greatly by the fluid motion.

We numerically simulated these conditions using a Navier-Stokes code which included surface shear and gravity. The computations were made on the CYBER 203 computer at NASA-Langley Research Center. The Prandtl number for the 1000 centistoke oil is 8570, which is the ratio of the vorticity diffusivity (kinematic viscosity) to the thermal diffusivity. This high ratio of diffusivities indicates that the vorticity (velocity) field will be diffused at a much higher rate than the temperature field. Thus, a quasi-steady velocity field will be established long before the equilibrium temperature field is established. Since the temperature field affects the velocity field through the surface shear boundary condition, the quasi-steady velocity field slowly changes while the temperature field approaches its steady state. This disparity in the two diffusivities creates a difficulty in the numerical computations. The integration time step, Δt , is given by

$$\Delta t = \frac{1}{2} \left(\frac{\Delta x^2}{\alpha + \nu} \right) \quad (4)$$

where Δx is the spacing distance between grid lines, α is thermal diffusivity and ν is vorticity diffusivity (kinematic viscosity). Thus, the integration time step is limited by the larger of the two diffusivities. In order to maintain stability, a very small time step is required for the coupled vorticity and thermal diffusion problem compared to what would be required for the thermal diffusion problem alone. Thus for a fully coupled solution, an extremely large number of integration time steps would be required to reach the steady state solution.

This numerical difficulty was dealt with by resorting to an alternating coupled-uncoupled solution technique. A fully coupled solution, using the

small time step required for the coupled solution, was used to bring the velocity field to a quasi-steady state condition. Then, holding the velocity field fixed, the temperature advection-diffusion equation was integrated at a much larger time step based on the thermal diffusivity. This procedure was alternated until convergence was achieved.

The results of the numerical integration are shown graphically in Figs. 1 through 4. These figures present, respectively, streamlines, absolute velocity contours, velocity vectors and temperature contours at steady state. The maximum computed velocity is about 0.05 mm/sec compared to the 0.07 mm/sec estimated from Eq. (1). The mid-temperature contour is shown to be distorted by about 4 percent of the distance across the free surface due to fluid motion, compared to the 8 percent predicted from Eq. (3).

The good agreement between the numerically computed results and estimates obtained by simple algebraic equations essentially verifies the accuracy of the computer program. Unfortunately, the computed velocities for this first set of conditions (1000 centistoke viscosity grade oil and 5 C temperature difference) are well below the 1 mm/sec experimental guidelines.

Referring to Eq. (3), we find that, at the minimum desirable fluid velocity of 1 mm/sec, the degree of distortion in the temperature contours is unacceptably high (greater than 100 percent). The problem lies in the extremely low thermal diffusivity of the silicone oil. At this point, we have arrived at a dilemma. It appears that we cannot have acceptably high fluid velocities without producing large distortions in the temperature field, using the silicone oil. If the silicone oil is used, then large distortions in the temperature field will have to be accepted and dealt with in the experimental program.

Several other sets of candidate experimental conditions were simulated to determine what effect the various parameters will have on the flow

velocities and temperature field. An extreme example is the case of the 10 centistoke viscosity grade fluid and 5 C temperature difference. Computer generated plots of streamlines, absolute velocity and temperature contours, and velocity vectors are shown in Figs. 5 through 8. Note the large distortions exhibited in these results compared to the symmetry in the results shown in Figs. 1 through 4. The high fluid velocities in the 10 centistoke oil resulted in large distortions in the temperature field. The distortions in the temperature field produced increased temperature gradients toward the downstream end of the free surface, which produced still higher surface shears and, hence, higher velocities. The velocity near the downstream end of the free surface, therefore, becomes much higher than the average across the surface, apparently creating the vortex shown in the streamline plot in Fig. 5. It would obviously be extremely difficult to accurately measure velocities in this kind of distribution.

We next tried 50 centistoke oil with a temperature difference of 2 C. These results are shown in Figs. 9, 10, and 11. The streamlines are shown in Fig. 9 to be much less distorted than in the 10 centistoke oil. The maximum velocity shown in Fig. 10 is about 1 mm/sec, which corresponds well with our experimental guidelines. Here again, however, the higher velocities are concentrated near the downstream end of the free surface, and the average velocities over the free surface are much lower. This is indicated also in the temperature distribution shown in Fig. 11.

As discussed earlier, the distortions in the velocity and temperature fields are due to the extremely low thermal diffusivity of the silicone oil. In order to provide an indication of the behavior of a higher thermal diffusivity fluid, we increased the thermal diffusivity of the 50 centistoke fluid by a factor of 20 and recomputed. The results are shown in Figs. 12 through 15. Note that the streamlines shown in Fig. 12 and velocity fields shown in Figs. 13 and 14 are nearly symmetrical. Also, the amount of distortion in the temperature contours is shown to be greatly reduced as compared to the normal thermal diffusivity silicone oil.

The next set of test conditions that we simulated was for the 50 centistoke fluid with a temperature difference of 0.5 C. We anticipated that this would produce velocities well below the experimental guidelines, and the temperature difference was also somewhat lower than desired from the experimental standpoint. The idea behind performing these simulations was to observe the amount of velocity and temperature field distortion for silicone oil at the extreme low end of the range of conceivably acceptable velocities. The results are shown in Figs. 16 through 19. The maximum velocity was found to be about 0.1 mm/sec, an order of magnitude below the experimental guidelines. The streamlines are shown in Fig. 16 to be slightly distorted. The velocity field is shown in Figs. 17 and 18 to increase continuously to a maximum at the downstream end of the free surface. The temperature field is shown in Fig. 19 to be considerably distorted even at the small fluid velocities observed for this case.

The final set of test conditions that we numerically simulated was for 20 centistoke oil with a temperature difference of 5 C. We anticipated that these conditions would result in acceptably high fluid velocities, but would display unacceptably high distortions in the temperature and velocity fields. These results are shown in Figs. 20 through 23 for zero gravity and in Figs. 24 through 27 with a downward directed gravitational force of 1 g imposed. The effect of gravity appears to be negligible. Note the severe distortion in the streamline, velocity and temperature fields. Surface velocities are essentially the same for both gravity conditions and are plotted in Fig. 28 as one curve. The surface velocities are shown to be relatively uniform at about 1 mm/sec over a large portion of the free surface. An extreme value of about 5 mm/sec is reached in a sharp peak near the downstream end.

Again, as an indication of what might be expected from a higher thermal diffusivity fluid, we increased the thermal diffusivity by a factor of 100, and repeated the computations for the 20 centistoke fluid with 5 C temperature difference. Computer generated plots are shown in Figs. 29 through 32.

These plots all show very little distortions in the velocity and temperature fields. The plot of surface velocity in Fig. 33 shows a smooth parabolic-like curve with a maximum velocity of about 2 mm/sec in the center of the free surface. Increasing the thermal diffusivity by a factor of 100 places it in the range of liquid metals, e.g., melted tin.

CONCLUSIONS

The thermocapillary convection experimental configuration was successfully numerically simulated over a wide range of possible test conditions. Some difficulty arose as a result of the extremely low thermal diffusivity of the silicone oil. First, the wide disparity between the vorticity and thermal diffusion rates resulted in extremely long convergence times in the numerical simulation. This difficulty was overcome by the use of alternating coupled and uncoupled numerical integrations of the mass, momentum and energy conservation equations. Second, the low thermal diffusivity was shown to result in undesirable distortions in the velocity and temperature fields. If these undesirable distortions are determined to be unacceptable, a higher thermal diffusivity fluid will be required.

REFERENCES

1. Robertson, S.J., L.W. Spradley, and M.P. Goldstein, "Manufacturing in Space: Fluid Dynamics Numerical Analysis," LMSC-HREC TR D697821, Lockheed Missiles & Space Company, Huntsville, Ala., August 1980.
2. Robertson, S.J., L.A. Nicholson, and L.W. Spradley, "Manufacturing in Space: Fluid Dynamics Numerical Analysis," LMSC-HREC TR D784480, Lockheed Missiles & Space Company, Huntsville, Ala., August 1981.
3. Robertson, S.J., L.A. Nicholson, and L.W. Spradley, "Manufacturing in Space: Fluid Dynamics Numerical Analysis," LMSC-HREC TR D867640, Lockheed Missiles & Space Company, Huntsville, Ala., September 1982.
4. Dow Corning Bulletin 05-145, February 1966.

Table 1 PROPERTIES OF SILICONE OIL

Density, ρ	0.971 gm/cm ³
Thermal Conductivity, k	0.00038 cal/cm-sec-C
Specific Heat, C	0.335 cal/gm-C
Volumetric Coefficient of Thermal Expansion, β_T	0.00096/C
Surface Tension, σ	21.2 dyne/cm
Surface Tension Temperature Coefficient, $d\sigma/dT$	-0.058 dyne/cm-C
Kinematic Viscosity, ν	Available in Wide Range of Viscosity Grades

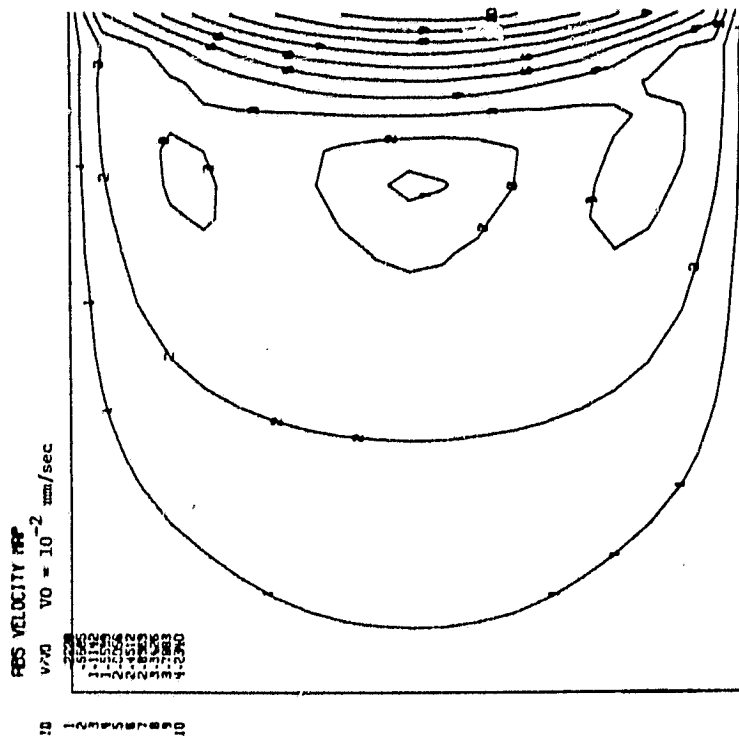


Fig. 2 Absolute Velocity Contour Plot for 1000 Centistoke Silicone Oil with Temperature Difference of 5 C

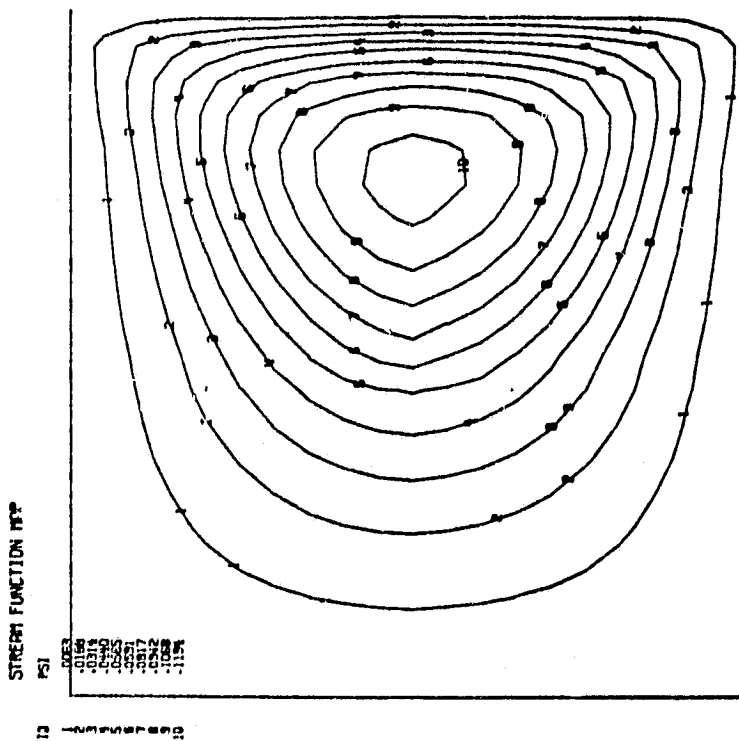


Fig. 1 Streamline Plot for 1000 Centistoke Silicone Oil with Temperature Difference at 5 C

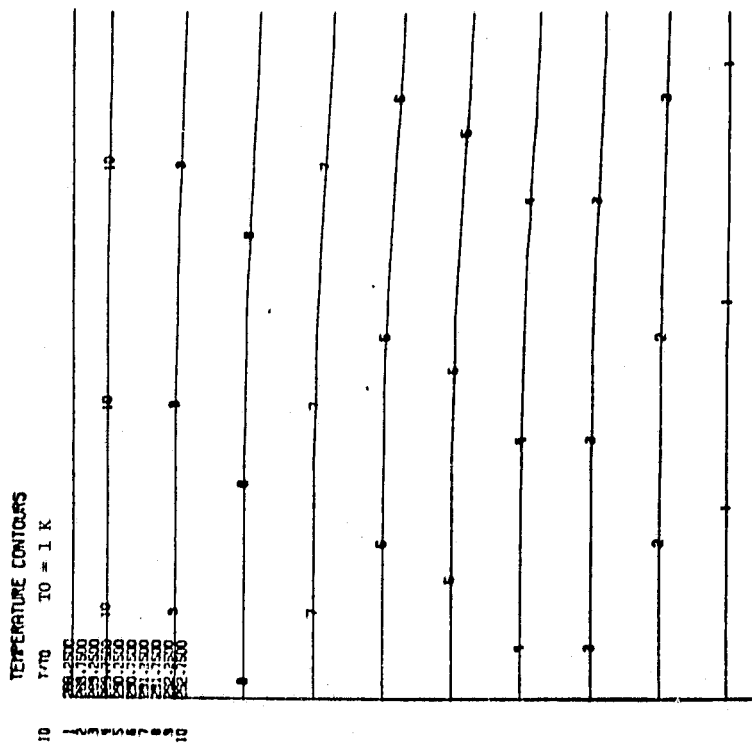


Fig. 3 Velocity Vector Plot for 1000 Centistoke Silicone Oil with Temperature Difference of 5 C

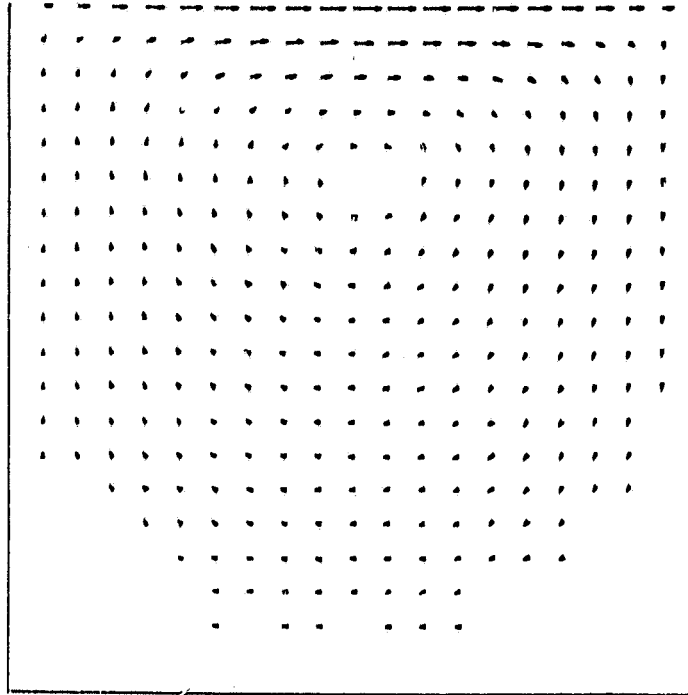


Fig. 4 Temperature Contour Plot for 1000 Centistoke Silicone Oil with Temperature Difference of 5 C

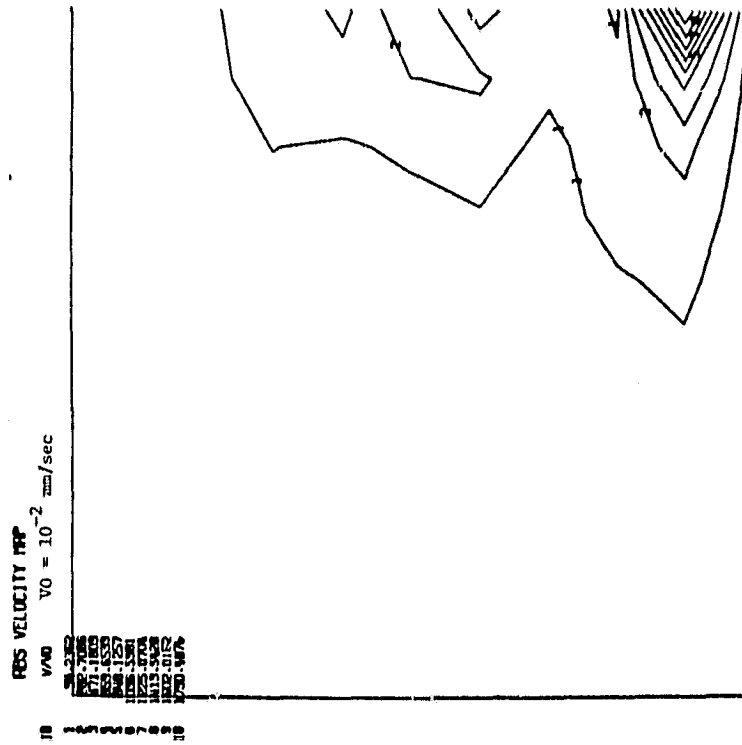


Fig. 5 Streamlines for 10 Centistoke
Silicone Oil with Temperature
Difference of 5 C

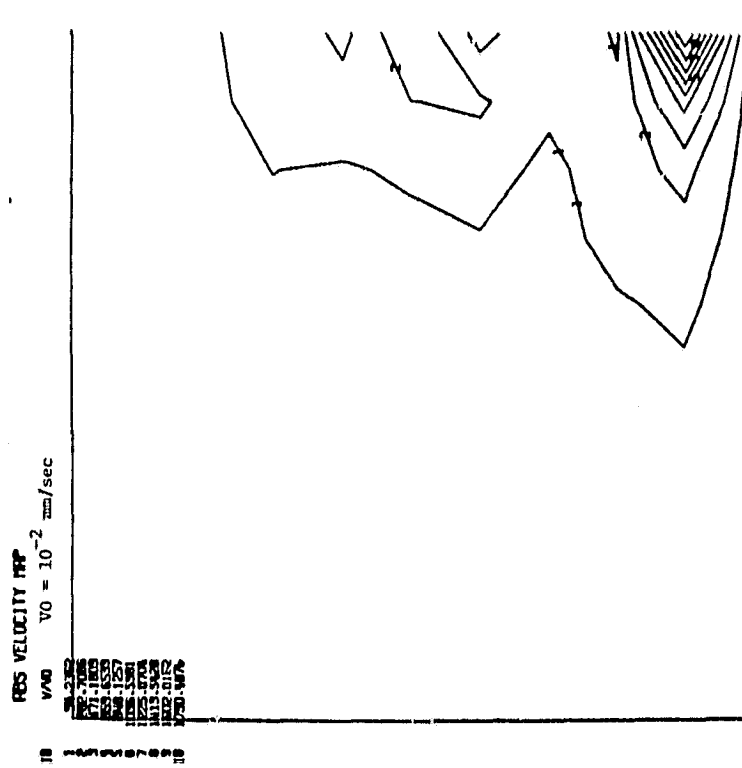
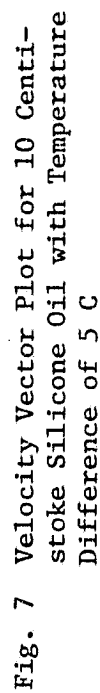
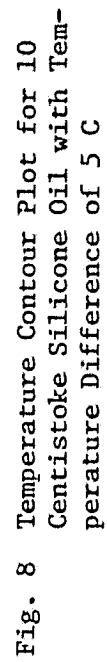
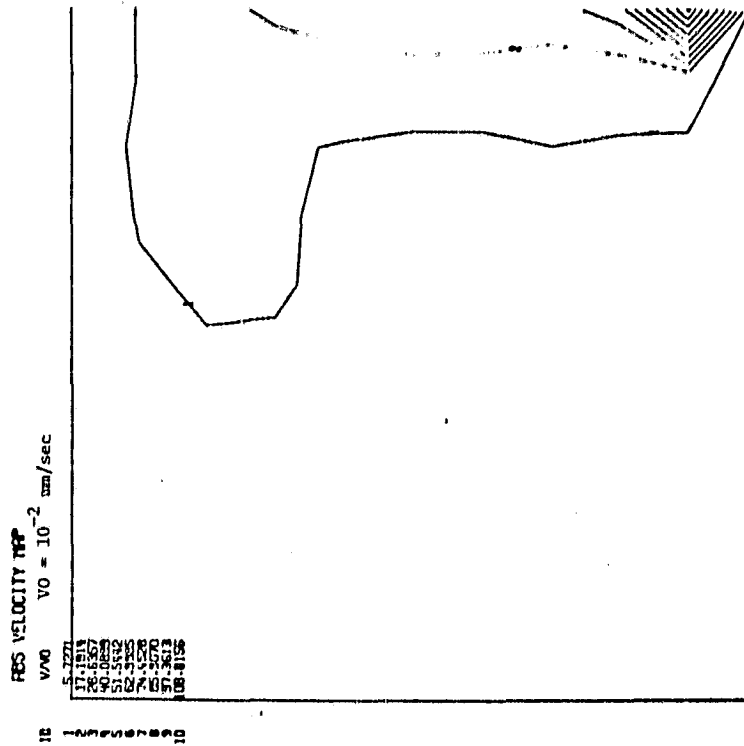


Fig. 6 Absolute Velocity Contour Plot for 10
Centistoke Silicone Oil with Tempera-
ture Difference of 5 C





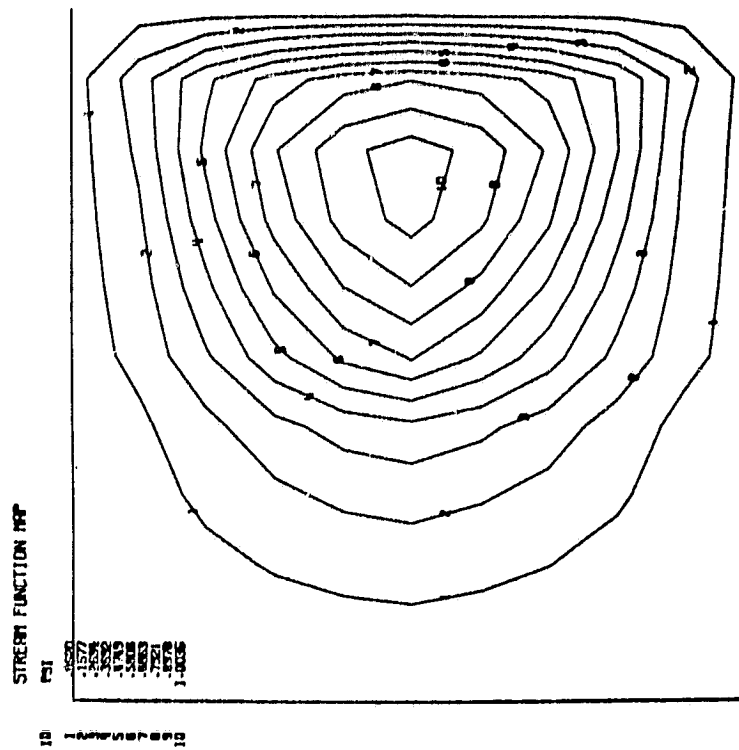


Fig. 12 Streamline Plot for 50 Centistoke Silicone Oil with Temperature Difference of 5 C and Thermal Diffusivity Increased by Factor of 20

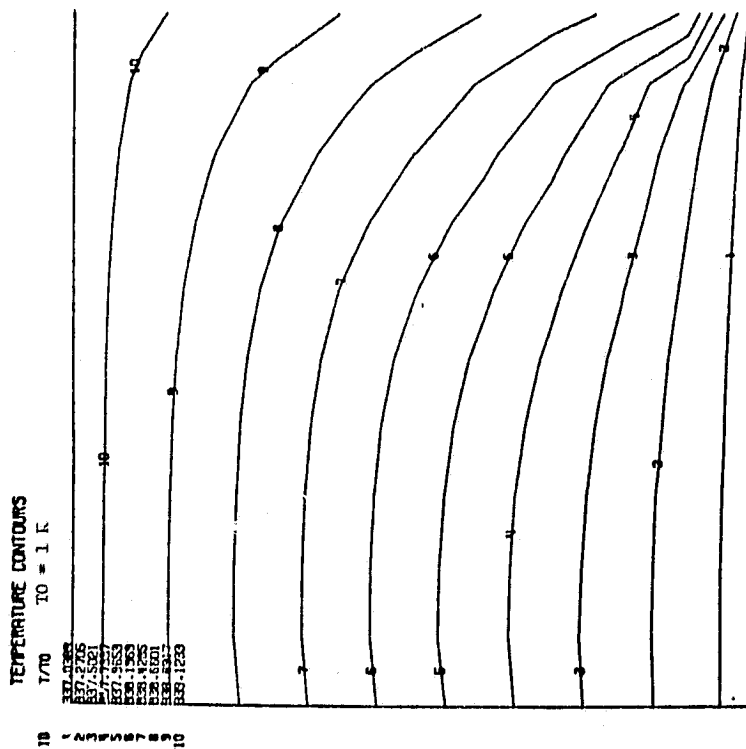
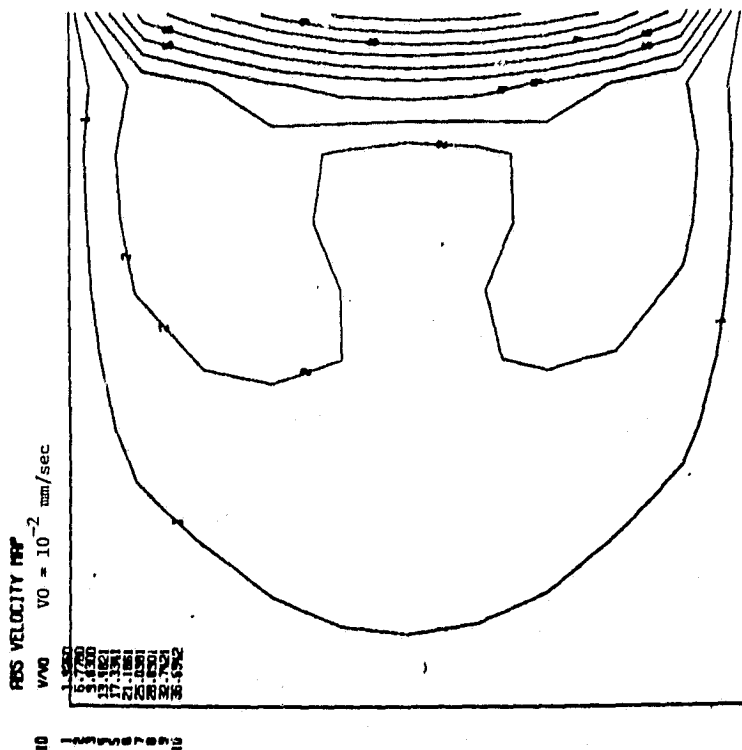


Fig. 11 Temperature Contour Plot for 50 Centistoke Silicone Oil with Temperature Difference of 2 C



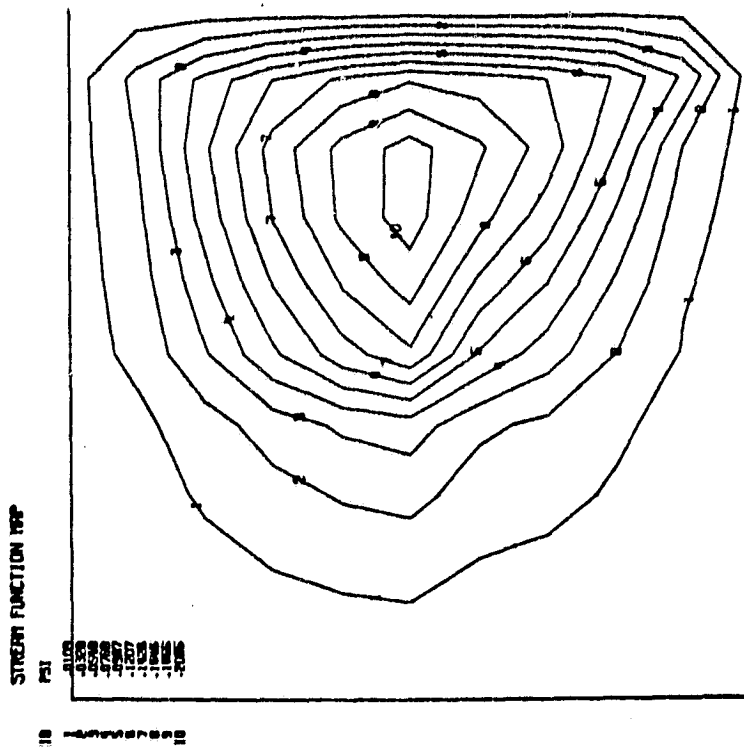


Fig. 16 Streamline Plot for 50 Centistoke Silicone Oil with Temperature Difference of 0.5 C

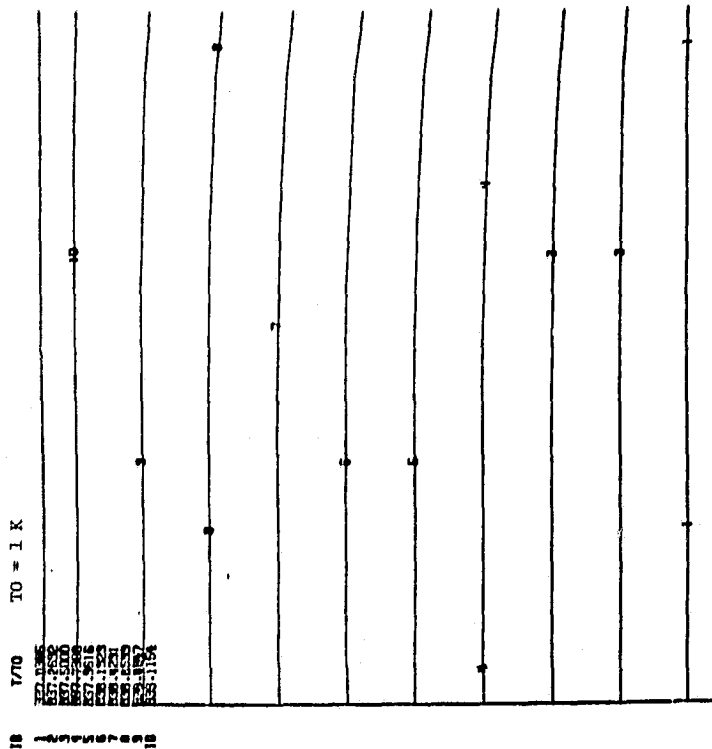


Fig. 15 Temperature Contour Plot for 50 Centistoke Silicone Oil with Temperature Difference of 5 C and Thermal Diffusivity Increased by Factor of 20

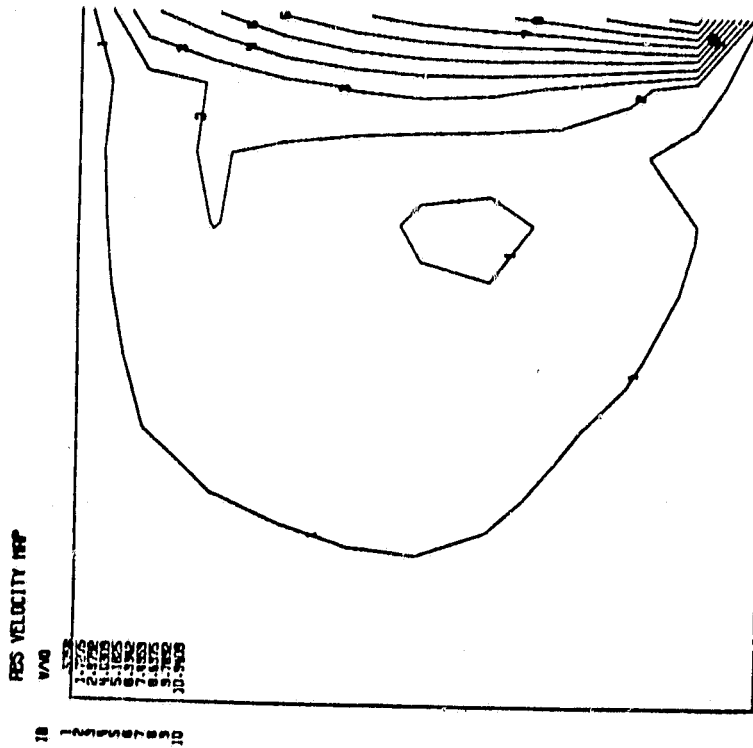


Fig. 17 Absolute Velocity Contour Plot for 50 Centistoke Silicone Oil with Temperature Difference of 0.5 C

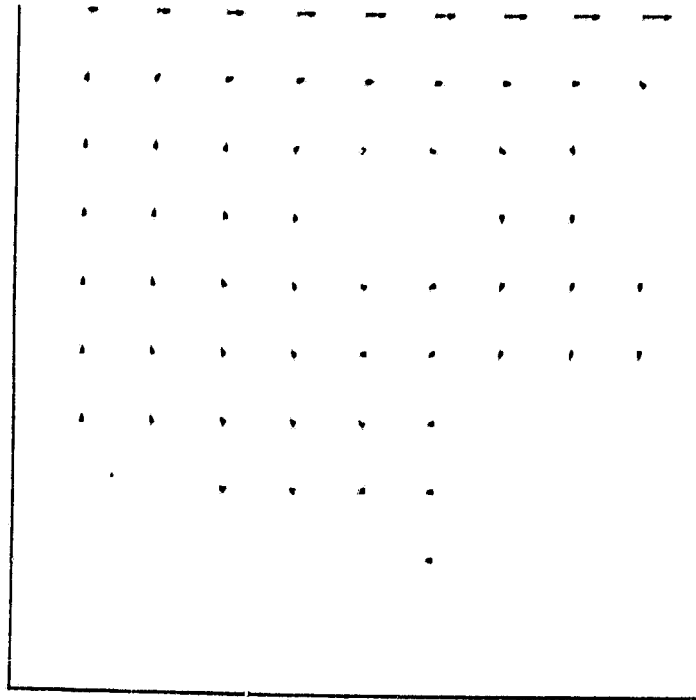
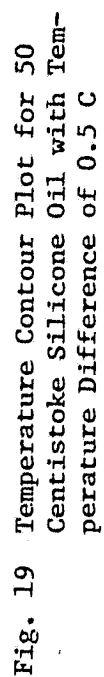
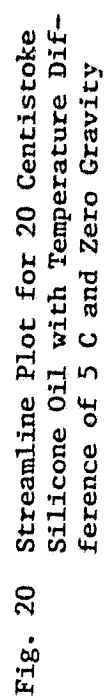


Fig. 18 Velocity Vector Plot for 50 Centistoke Silicone Oil with Temperature Difference of 0.5 C



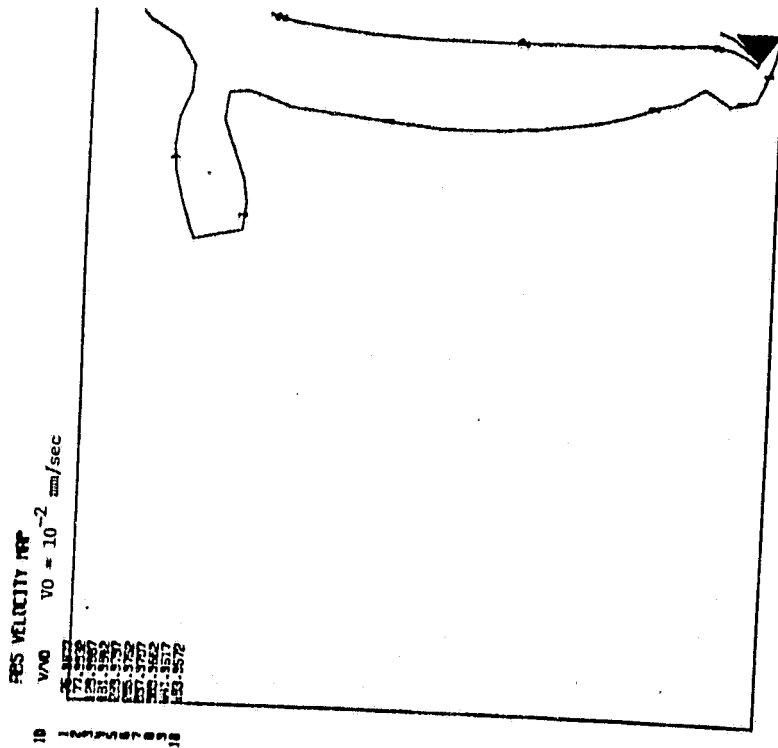


Fig. 21 Absolute Velocity Contour Plot for 50 Centistoke Silicone Oil with Temperature Difference of 5 C and Zero Gravity

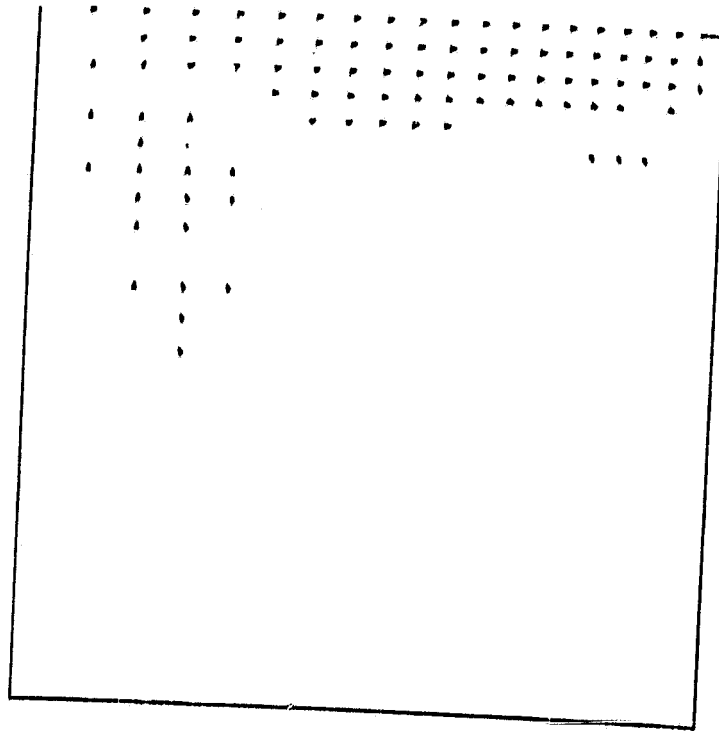


Fig. 22 Velocity Vector Plot for 20 Centistoke Silicone Oil with Temperature Difference of 5 C and Zero Gravity

ORIGINAL PAGE 19
OF POOR QUALITY

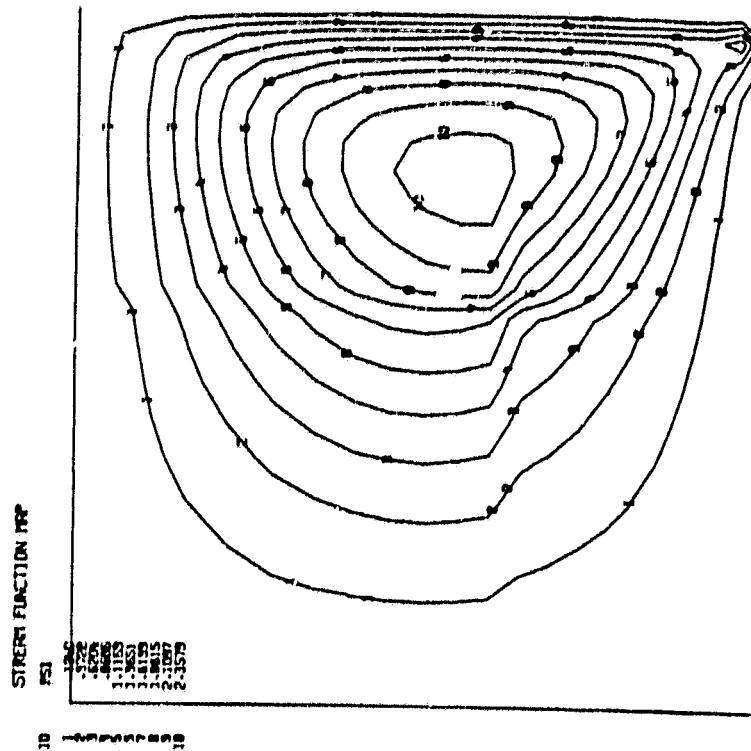


Fig. 24 Streamline Plot for 20 Centistoke Silicone Oil with Temperature Difference of 5 C and 1 g Gravity

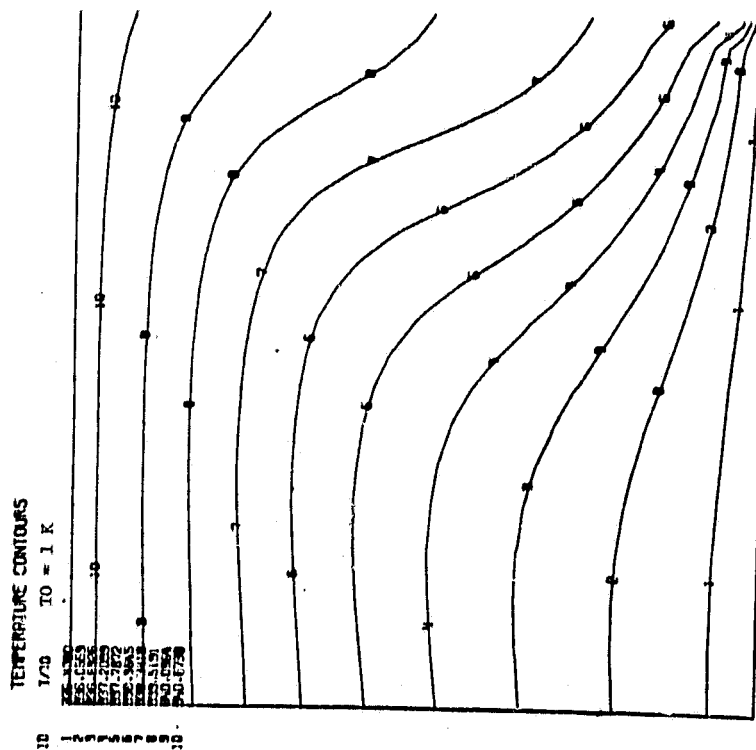


Fig. 23 Temperature Contour Plot for 20 Centistoke Silicone Oil with Temperature Difference of 5 C and Zero Gravity

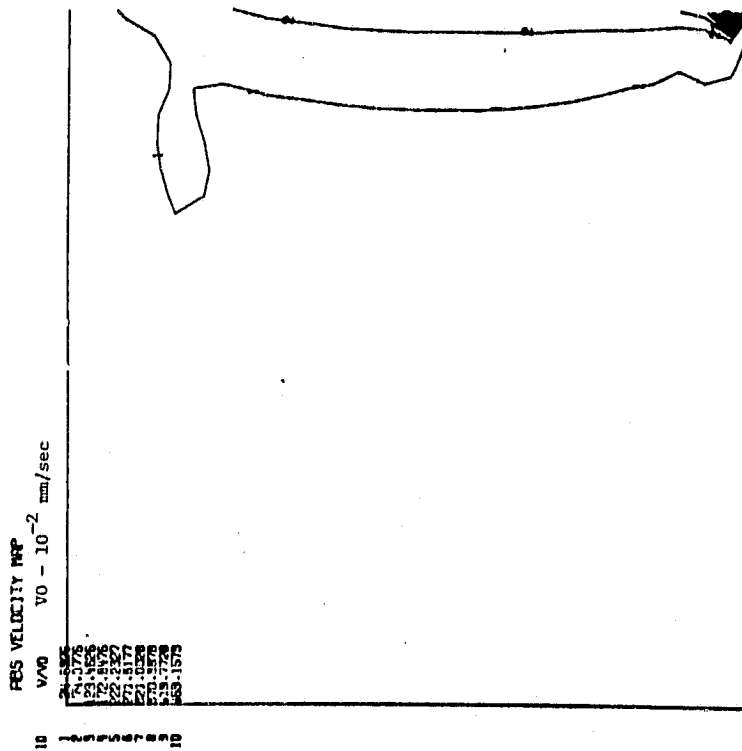


Fig. 25 Absolute Velocity Contour Plot for 20 Centistoke Silicone Oil with Temperature Difference of 5 C and 1 g Gravity

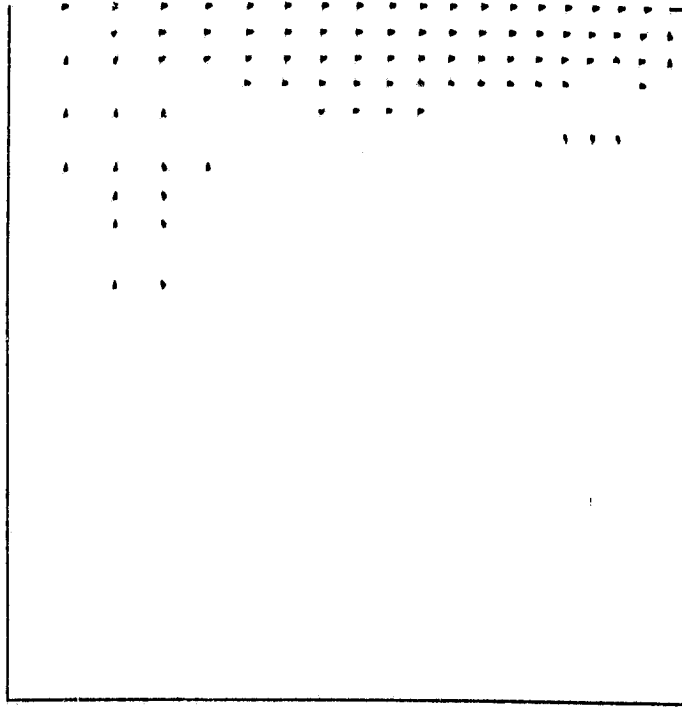
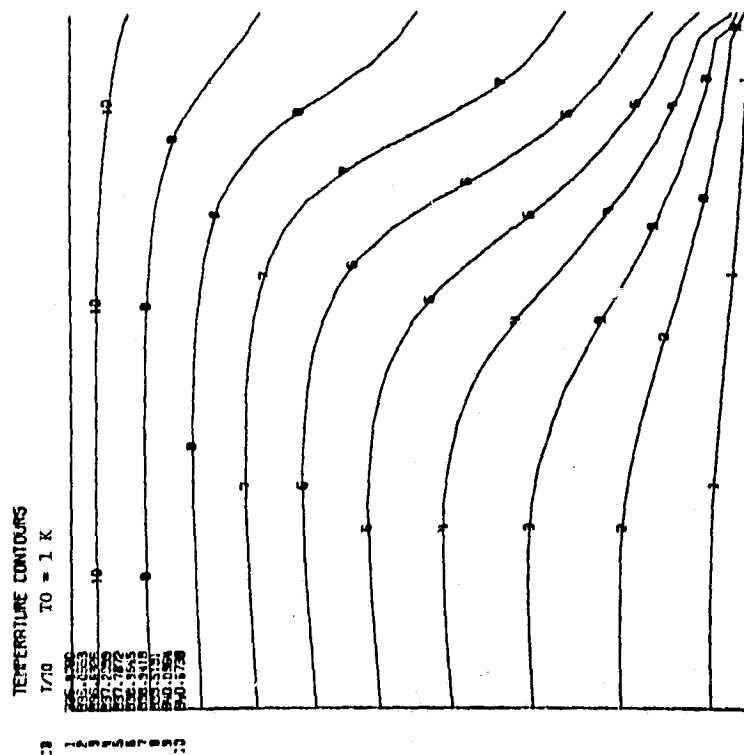


Fig. 26 Velocity Vector Plot for 20 Centistoke Silicone Oil with Temperature Difference of 5 C and 1 g Gravity



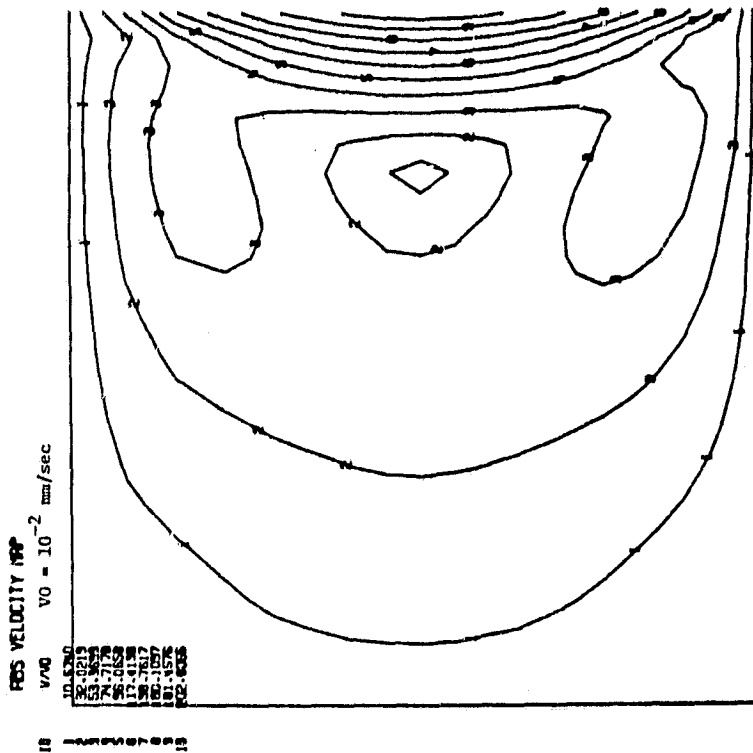
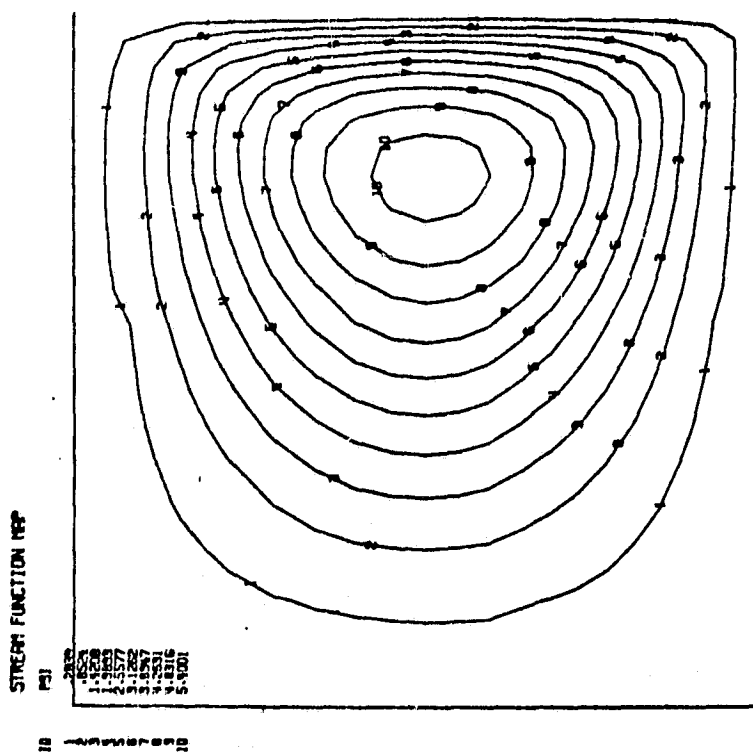


Fig. 30 Absolute Velocity Contour Plot for 20 Centistoke Silicone Oil with Temperature Difference of 5 C and Thermal Diffusivity Increased by Factor of 100



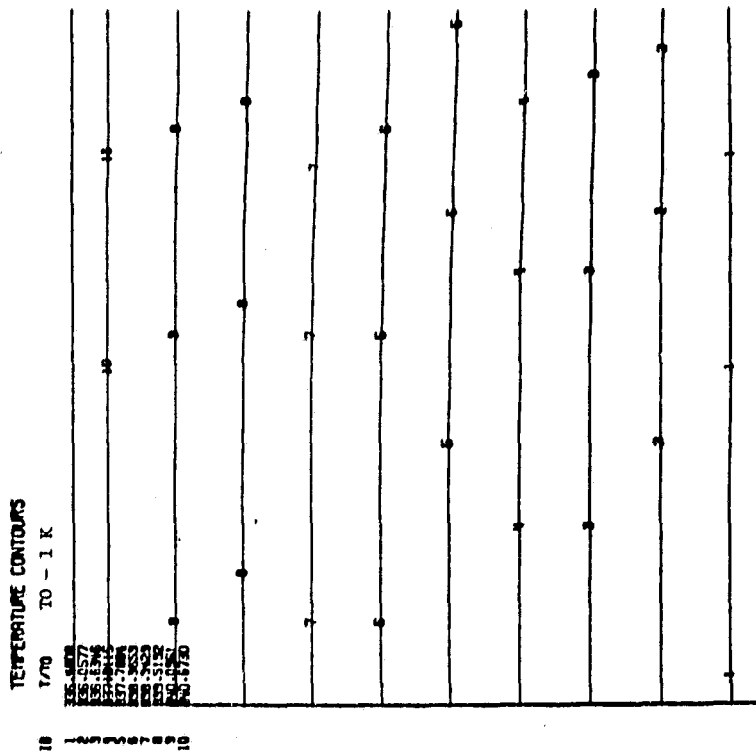


Fig. 32 Temperature Contour Plot for 20 Centistoke Silicone Oil with Temperature Difference of 5 C and Thermal Diffusivity Increased by Factor of 100

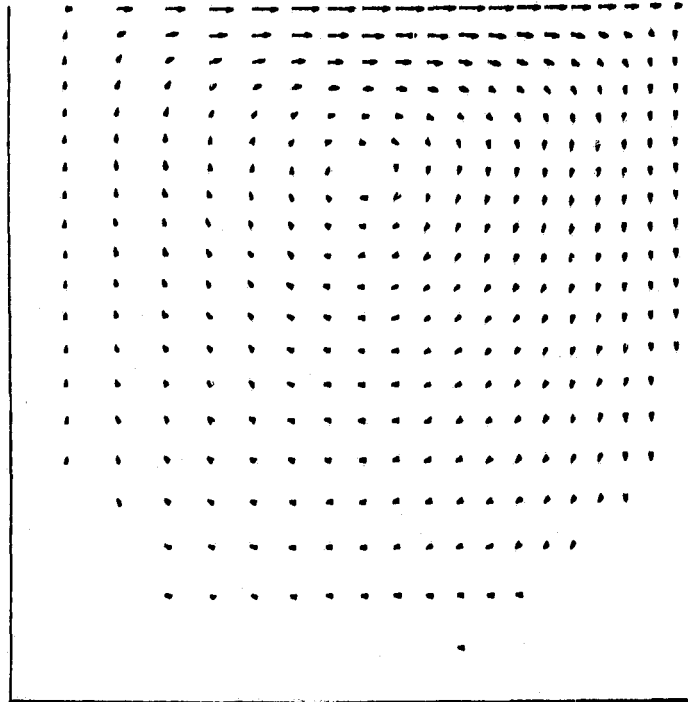


Fig. 31 Velocity Vector Plot for 20 Centistoke Silicone Oil with Temperature Difference of 5 C and Thermal Diffusivity Increased by Factor of 100

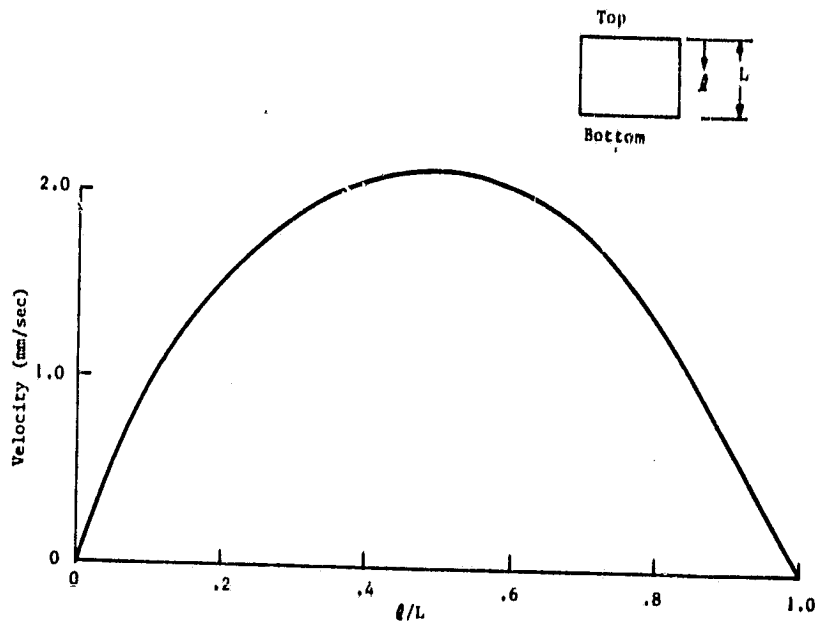


Fig. 33 Velocity Along Free Surface for 20 Centistoke
Silicone Oil with Temperature Difference of
5 C and Thermal Diffusivity Increased by
Factor of 100

Appendix
SIMPLIFIED ANALYTICAL MODEL
FOR ESTIMATING MARANGONI
CONVECTION IN SQUARE ENCLOSURES

Appendix

We assume simple algebraic forms for the velocity components:

$$u = U(x) \sin(2\pi \frac{y - L/2}{L}) \quad (A.1)$$

$$v = V(x) \cos(\pi \frac{y - L/2}{L}) \quad (A.2)$$

These equations provide the general circulatory flow pattern that we expect from intuition. The conservation of momentum in the y direction is expressed by the following differential equation:

$$\frac{\partial}{\partial x} (\rho uv - \tau) + \frac{\partial}{\partial y} (\rho v^2 + p) = 0 \quad (A.3)$$

After dropping insignificant terms, substituting $\tau = \mu \partial v / \partial x$, and using the form of v given by Eq. (A.2), this becomes:

$$\mu \frac{\partial^2 v}{\partial x^2} \cos(\pi \frac{y - L/2}{L}) = \frac{\partial p}{\partial y} \quad (A.4)$$

Integrating this equation with respect to x along $y = L/2$, with the boundary conditions, $v = 0$ at $x = 0$ and $\tau_w = \mu \partial v / \partial x$ at $x = L$, yields:

$$v = \frac{1}{\mu} \{ \tau_w - \frac{\partial p}{\partial y} (L - \frac{x}{2}) \} x \quad (A.5)$$

ORIGINAL PAGE 13
OF POOR QUALITY

This equation automatically satisfies force balances on the overall system in the y-direction, but it contains the unknown $\partial p / \partial y$. This is removed by satisfying a mass balance along $y = L/2$:

$$\int_0^L v \, dx \Big|_{y=L/2} = 0 \quad (A.6)$$

This results in

$$\frac{\partial p}{\partial y} = \frac{3}{2L} \tau_w \quad (A.7)$$

Combining Eqs. (A.2), (A.5), and (A.7) results in the expression for the v-component of velocity:

$$v = \frac{\tau_w L}{2\mu} \left(\frac{3}{2} \frac{x}{L} - 1 \right) \frac{x}{L} \cos\left(\pi \frac{y - L/2}{L}\right) \quad (A.8)$$

with the maximum v-component velocity, v_{\max} , being at the free surface ($x = L$) and given by

$$v_{\max} = \frac{\tau_w L}{4\mu} \quad (A.9)$$

Note that, for $\tau_w > 0$, v is negative for $x < 2/3 L$, positive for $x > 2/3 L$ and, of course, zero at $x = 2/3 L$. The general flow, therefore, obviously is counterclockwise around the point $x = 2/3 L$ and $y = L/2$. Mass conservation requires that:

$$\int_{2/3 L}^L v \, dx \Big|_{y=L/2} = \int_{1/2 L}^L u \, dy \Big|_{x=2/3 L} \quad (A.10)$$

We assume $U(x)$ in Eq. (A.1) to be of the form

$$U = A(1 - \frac{x}{L}) (\frac{x}{L})^2 \quad (A.11)$$

This provides an extreme value for v at $x = 2/3 L$ and zeros at $x = 0$ and L .
Carrying out the integrations in Eq. (A.10) yields

$$A = -\frac{\pi}{4} \frac{\tau_w L}{\mu} \quad (A.12)$$

Combining Eqs. (A.1), (A.11), and (A.12) yields the expression for the u -component of velocity:

$$u = -\frac{\pi}{4} \frac{\tau_w L}{\mu} (1 - \frac{x}{L}) (\frac{x}{L})^2 \sin(2\pi \frac{y - L/2}{L}) \quad (A.13)$$

with the maximum u -component velocity, u_{\max} , being at $x = 2/3 L$ and $y = \frac{L}{2} (1 \pm \frac{1}{2})$ and given by

$$u_{\max} = \frac{\pi}{27} \frac{\tau_w L}{\mu} = \frac{4\pi}{27} v_{\max} \quad (A.14)$$

The temperature field may be represented by

$$T(x,y) = \bar{T}(y) + T'(x,y) \quad (A.15)$$

where \bar{T} is the temperature field for the fluid at rest and T' is the perturbation due to fluid motion.

The fluid-at-rest temperature distribution is given by

$$\bar{T} = T_o + \frac{\Delta T}{L} (y - L/2) \quad (A.16)$$

ORIGINAL PAGE 19
OF POOR QUALITY

where T_0 is the mid-point or average fluid temperature and ΔT is the temperature difference across the fluid.

We assume T' to be of the form

$$T' = B \left[\left(1 - \frac{2}{3} \frac{x}{L}\right) \left(\frac{x}{L}\right)^2 - \frac{1}{6} \right] \cos\left(\pi \frac{y - L/2}{L}\right) \quad (A.17)$$

This provides for the proper boundary conditions $\partial T'/\partial x = 0$ at $x = 0$ and L , and $T' = 0$ at $y = 0$ and L . It also results in

$$\int_0^L \int_0^L T' dx dy = 0 \quad (A.18)$$

This maintains the original average fluid temperature T_0 . We find the factor B by requiring the satisfaction of the advection-diffusion equation at the free surface mid-point ($x = L$ and $y = L/2$):

$$u \frac{\partial T}{\partial x} + v \frac{\partial T}{\partial y} = \alpha \left(\frac{\partial^2 T}{\partial x^2} + \frac{\partial^2 T}{\partial y^2} \right) \quad (A.19)$$

After inserting the values of u , v and the T derivatives at $x = L$ and $y = L/2$, we find

$$B = - \frac{1}{2(1 + \pi^2/12)} \frac{v_{\max} L}{\alpha} \Delta T \quad (A.20)$$

The expression for the temperature field then becomes

ORIGINAL PAGE 19
OF POOR QUALITY

$$T = T_o + \frac{\Delta T}{L} \left(y - \frac{L}{2}\right) + \frac{1}{8(1 + \pi^2/12)} \frac{\tau_w L^2}{\mu\alpha} \Delta T$$

$$\times \left[\left(1 - \frac{2}{3} \frac{x}{L}\right) \left(\frac{x}{L}\right)^2 - \frac{1}{6} \right] \cos\left(\pi \frac{y - L/2}{L}\right) \quad (A.21)$$

By setting the temperature T in Eq. (A.21) equal to the fluid-at-rest mid-point temperature T_o , the displacement, $\delta y = y - L/2$, of the mid-isotherm at the free surface ($x = L$) is found to be:

$$\frac{\delta y}{L} = \frac{1}{4(12 + \pi^2)} \frac{\tau_w L^2}{\mu\alpha}$$

$$= \frac{1}{12 + \pi^2} \frac{v_{\max} L}{\alpha} \quad (A.22)$$